We are IntechOpen, the world's leading publisher of Open Access books Built by scientists, for scientists

6,900
Open access books available

186,000
International authors and editors

200M
Downloads

Our authors are among the

154
Countries delivered to

TOP 1%
most cited scientists

12.2%
Contributors from top 500 universities

WEB OF SCIENCE™

Selection of our books indexed in the Book Citation Index in Web of Science™ Core Collection (BKCI)

Interested in publishing with us?
Contact book.department@intechopen.com

Numbers displayed above are based on latest data collected.
For more information visit www.intechopen.com

Chapter 12

ISOPerm: Non-Contacting Measurement of Dielectric Properties of Irregular Shaped Objects

Henning Mextorf, Frank Daschner, Mike Kent and Reinhard Knöchel

Additional information is available at the end of the chapter

http://dx.doi.org/10.5772/55079

1. Introduction

A mere glance at the contents of any of the conferences organised by ISEMA (International Society for Electromagnetic Aquametry) [1] shows that the measurement and control of water (its quantity and states) in materials is a very wide and active field. That water lends itself to study in this way is because of its very dominant dispersive dielectric properties and an unusually large dipole moment for such a small molecule (1.84 Debye units). At room temperature the dispersion is centred on $\sim$ 12.5GHz and the real part of the relative permittivity at its upper and lower frequency extremes is $\sim$ 4.3 and 80 respectively [2]. The complex dielectric properties characteristic of this dispersion are the properties that are measured and correlated with whatever aspect of the water content is of interest. Historically much of the work was carried out at one or two frequencies, mostly in X-band where the dielectric loss is at a maximum, but the advent of time domain reflectometry (TDR) [3] for broadband dielectric measurements in the microwave region eventually led to such measurements being made using open ended coaxial sensors [4], although a greater potential of such measurements was only realised later by the authors. The use of such sensors freed the experimenter from the difficult task of defining the sample shape by means of a sample cell; the measurements still required however that the sensor be in contact with the sample. As a true frequency domain UWB application, dielectric measurements of foodstuffs over a wide range of frequencies (100MHz to 20GHz) were made using network analysers and such coaxial sensors [5, 6]. Drawing on the experience in other chemometric applications such as NIR (near infra-red spectroscopy) [7], the dielectric spectra obtained were subjected to various multivariate analyses (PCR (principal component regression), PLSR (partial least squares regression), and ANNs (artificial neural networks both linear and non-linear)). Such analyses both compress the data into orthogonal factors and extract from those factors the best information to predict the composition of the foodstuffs. In such analysis the important variables are, not so much the dielectric properties at each sampled frequency, but rather the shape of the spectrum. In effect the data reduction provides suitable shape descriptors, which are in the case of foods, very dependent on the water content and its interaction with other

INTECH
open science | open minds

©2013 Mextorf et al., licensee InTech. This is an open access chapter distributed under the terms of the Creative Commons Attribution License (http://creativecommons.org/licenses/by/3.0), which permits unrestricted use, distribution, and reproduction in any medium, provided the original work is properly cited.

constituents such as proteins and carbohydrates. Any that are dependent on other factors are eliminated in the regression analysis having no significant correlation with the material properties. Rather than using measurements in the frequency domain, of course it is possible to transform time domain measurements to the frequency domain using Fourier or other forms of transformation. For time varying data acquired by TDR the inverse Fourier transform in its most general form can be written as in equation 1.

$$h(t) = \frac{1}{2\pi} \int_{-\infty}^{+\infty} g(f) e^{2\pi i f t} \mathrm{d}f, \tag{1}$$

where h(t) is a time dependent function the Fourier transform of which is a frequency dependent spectrum g(f). Examination of equation (1) shows that at any instant t every component part of the spectrum contributes to the value of h. Because the subsequent multivariate analysis can be thought of as dealing with shape and is concerned only with the variations in g then transformation of h(t) to the frequency domain is not required, since related variations are present in h(t) and the shape of the time domain function is equally useful. A further justification for eliminating the transformation step concerns the difficulties with which it is fraught. Firstly, the truncation of the pulse after a finite measurement interval can introduce undesirable distortions in the integral from convolution of the pulse with the rectangular time window (windowing). Secondly, the act of sampling the pulse at regular intervals means that frequencies present with periods shorter than the sampling interval are incorporated as lower frequency information (aliasing), and thirdly, to accurately reconstruct the reflection coefficients in the frequency domain exact time referencing of the pulse is required, else phase errors cause large inaccuracies at the high frequency end of the spectrum. By carrying out the analysis on the raw, sampled TDR pulse, all the errors above can be avoided. This was tried and demonstrably gave the same results as the spectral data, with less computer effort and fewer error generating problems. The first problem to which this was applied was something less tangible than water content: it was in fact the quality of various seafoods as defined by more subjective methods [8]. The success of this approach naturally led to attempts to measure dielectric objects in a non-contacting fashion, using firstly transmitted UWB quasi-Gaussian pulses of 400ps width [9]. The transmitting and receiving antennas in this initial work were double ridged horns and the sample was arranged in a wide layer of uniform thickness. In such a situation, additional interfering variables can be the position of the antennae, polarization of the transmitted wave, multiple path effects and a host of others, all of which may be eliminated by multivariate analysis. Effects due to dielectric properties can be separated from those due to geometry and other exterior factors. Thereafter, further work followed with samples of increasingly complex shapes and different orientations, beginning with simple rectangles and progressing to other shapes such as triangles and circles [10, 11], albeit still of constant thickness. At the same time, various forms of UWB antennas were investigated but currently the choice is an array of simple dipoles for the receiving antennas with a horn antenna transmitting the pulse. The multivariate data analysis still uses PCA as a first step to reduce the data and provide shape descriptors, but because PCR is not entirely suitable for non-linear processes (being a linear regression of variables) the PCs are used as input to a non-linear ANN. A great deal of work has now been done, gradually broadening the application parameters until now it is possible to measure UWB dielectric properties of objects with any shape, thickness, orientation and without contact [12–20]. This has been the subject of the project 'ISOPerm' (irregularly shaped objects-permittivity) the methods and results of which will now be described.

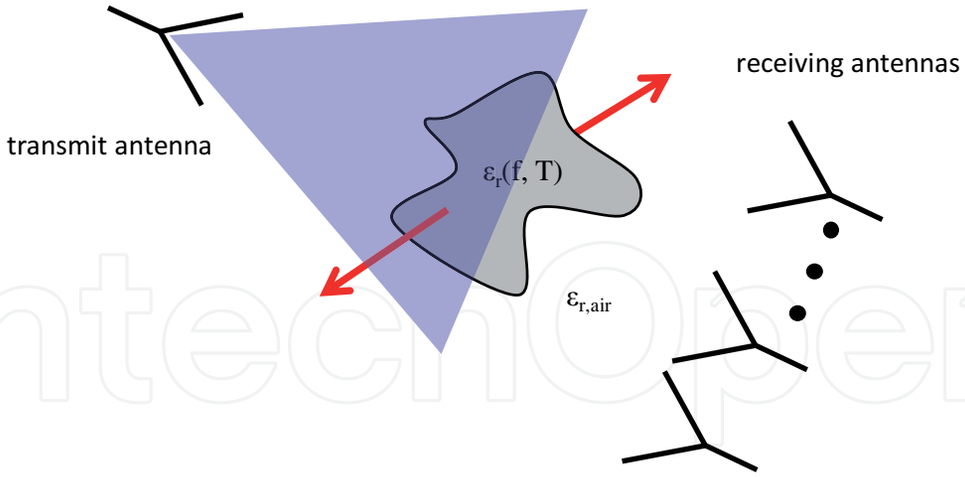

Figure 1. Irregularly shaped object illuminated by an electromagnetic wave.

2. Problem and approach

There is no appropriate method for the determination of the dielectric or related properties of irregular shaped objects in free-space. The investigated objects are considered to be small compared to the range of wavelengths and the footprints of the antennas used. A visualization of the problem is depicted in Figure 1. An electromagnetic wave illuminates an irregularly shaped object with its frequency and temperature dependent dielectric properties. It is surrounded by air. Portions of the scattered field are collected by multiple field probes, i.e. a line array of receiving antennas. The scattered signals contain information about geometry as well as the dielectric properties. Because of the complexity of the problem it is assumed that the development of a physical model (as used in conventional free-space methods having a plane parallel plate) would be too complex. Furthermore, an on-line method suitable for characterizing many objects in a short time is anticipated. Therefore, multivariate calibration methods are applied in order to separate dielectric from geometric influences. The objects are considered to be homogeneous and non-magnetic ($\mu_r = 1$). However, it is assumed that it would also be possible to predict both average permittivity and permeability. In research and industrial applications other properties, for example the water content, moisture, freshness or quality of foodstuffs, are of great interest. They are often strongly correlated to dielectric properties and can be determined directly without knowing the permittivity.

3. Measurement system and dedicated hardware

A measurement system has been built in order to verify the approach. Particular components, like the UWB-antennas used and the working principle of the whole set-up, are discussed in this section. A dedicated time domain transmission oscilloscope is presented. It is capable of transmitting and receiving UWB pulses with several gigahertz of bandwidth. It is specially tailored to the measurement problem and therefore functions with less hardware and software, is far more compact, and is cheaper compared to a universal laboratory instrument.

3.1. Compact ultra-wideband antennas and arrays

The sensor system should be able to transmit and receive ultra-wideband (UWB) signals in two orthogonal polarizations. This is of great importance if the orientation of the object

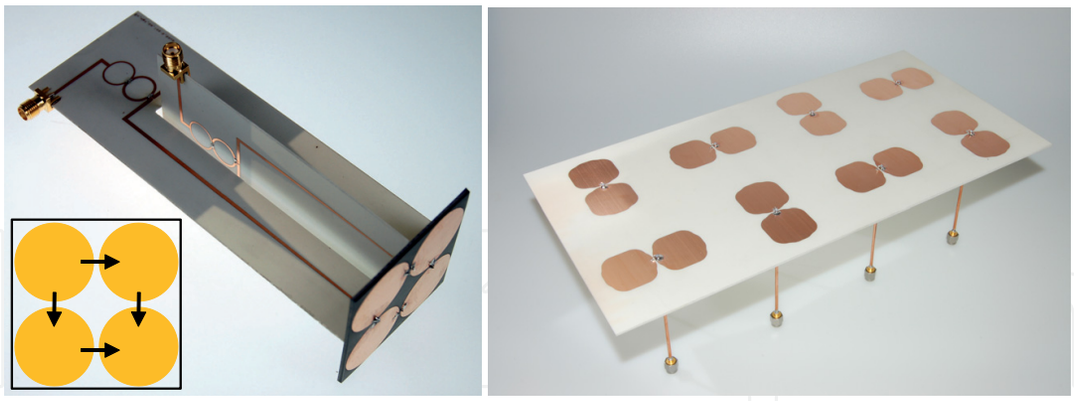

(a) Dual polarised dipole. (b) Dual polarised array.

Figure 2. Ultra-wideband antenna structures.

under test (e.g. prolate ellipsoid) is not known. There are several polarization set-ups for receiving co- and cross-polarized parts of the scattered wave. In the set-up used latterly the polarization of the transmitting antenna is tilted at 45° with respect to the receiving array so that ideally, without an object under test, the receiving antennas receive the transmitted pulse in equal proportions for each polarization. Therefore, dual orthogonal UWB antennas have been developed. Furthermore the single antennas should be as compact as possible while operating in the lower gigahertz range. The arrays presented later are not group antennas as commonly used. The received signal of every antenna is sampled separately in order not to confound the information at different locations with respect to the object under test. Operating at frequencies in the lower GHz range is anticipated because the electromagnetic waves have a higher penetration depth (especially for lossy dielectrics with a high permittivity) and therefore will be more affected.

There are many UWB antennas suitable for building dual polarized antennas [21–25]. Dual polarized dipole (see [26–31]) and horn antennas (see [32–35]) can already be found in the literature. Most of these antennas have the disadvantage that they have crossed feed points. It is possible to overcome this problem with the configuration depicted in Figure 2. Both the four radiation elements and the whole configuration are two-fold symmetric. Two dipoles are excited in even mode in horizontal as well as in vertical polarization. Ideally, due to the symmetry, both planes are decoupled. The diameter of the radiation elements is 24mm; the whole PCB containing the four radiating elements measures 50mm × 50mm. The antenna is equipped with two orthogonal feed networks; each is composed of a two stage Wilkinson divider and two tapered baluns. The horizontal and vertical polarization feed networks have dimensions of 50mm × 142mm and 50mm × 103mm, respectively. In order to avoid backward radiation, absorber material is mounted appropriately (the absorber material was removed for the photograph shown in Figure 2).

The matching at both ports is better than 7dB in a frequency range from 2GHz to 5.7GHz; the isolation is better than 30dB. At 5GHz the radiated crosspolar portion is suppressed by more than 25dB (boresight); the gain is 5.2dB. Measurements with a line containing four of these antennas lead to excellent results but the whole antenna structure is rather complex. Since a scenario with an object moving orthogonally to the line array is anticipated (e.g. a conveyor belt), a simpler arrangement can be used. The antenna array shown in Figure 2 consists of eight single linear broadband dipoles. The geometry is optimized regarding the

antenna matching. The radiating elements have a maximum diameter of 30mm. The feed is provided through a coaxial-slotline transition, so that no other components are necessary. The distance between two dipoles having an equal polarization is 80mm in each direction; between dipoles with the same polarization it is $\sqrt{2} \times 80$mm. The dimensions are overall 160mm $\times$ 320mm $\times$ 100mm. The matching is better than 10dB between 1.6GHz and 4.2GHz. The crosstalk between the single elements is maximum -20dB at 10GHz.

3.2. Signal generation and sampling

The core of the measurement system is the signal generation and sampling. The requirements for the system are that the step signals generated have a rise time in the range of 100ps, and a large amplitude. These signals are transmitted through the measurement path after which, the step response has to be sampled. The system should have a high bandwidth, low noise and low jitter. Furthermore it should be as compact and affordable as possible. Therefore, an impulse technique using equivalent time sampling is the method of choice. Classical swept sine wave techniques, as used in network analysers or real time digital sampling oscilloscopes, are too expensive, complex, and bulky.[1]

Equivalent time sampling is based on the repetitive stimulation by a measurement signal with a cycle duration of T_0. At every repetition of the measurement signal the moment of sampling is shifted by ΔT. The cycle of the sampling clock is then $T_1 = T_0 + \Delta T$. The sampled signal is therefore stretched to $T_2 = \frac{T_0}{\Delta T} T_1$. The effort regarding analog-to-digital conversion and the data transport and storage is greatly reduced compared to a real time oscilloscope. This technique has been used for decades; with recently available MMICs, both high performance and cheap hardware can be achieved. It is the method of choice for the sampling of signals with huge bandwidth in the GHz range with a high resolution. Laboratory instruments employing this technique have been used for preliminary investigations. In order to demonstrate the system performance and accuracy under practical conditions, dedicated hardware was developed. Two specially tailored systems were investigated. They differed

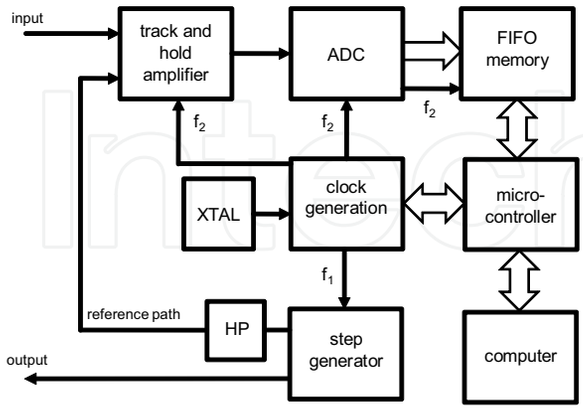

(a) Block diagram.

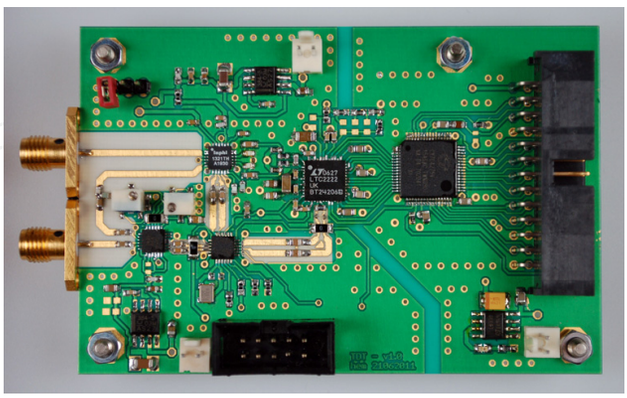

(b) Prototype: integrated on one PCB except microcontroller and computer.

Figure 3. Time domain transmission measurement system with a microcontroller.

[1] A rather exotic concept employing M-sequences can be found in this book (see chapter HALOS). There are also measurements carried out with this method which lead to excellent results [20].

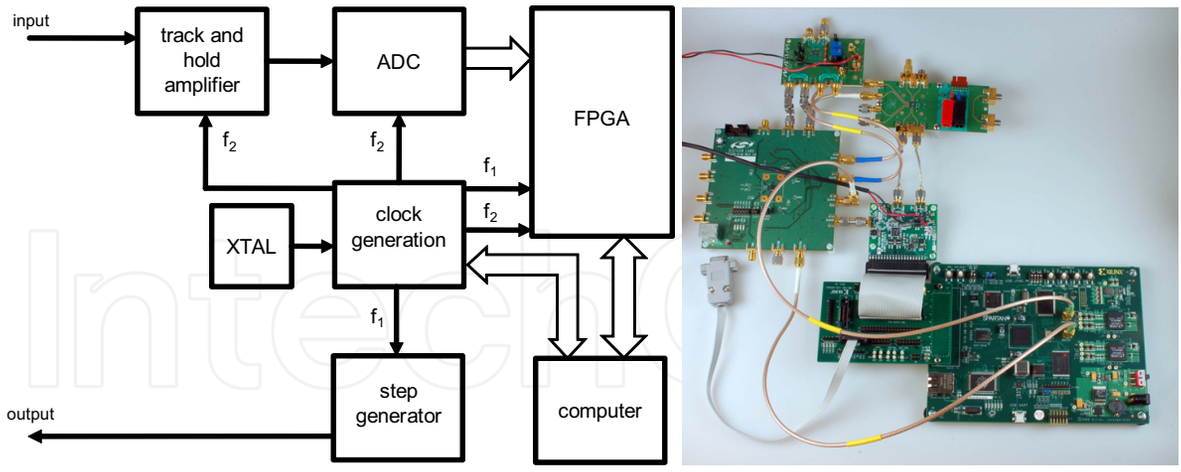

(a) Block diagram.

(b) Prototype: modular system except computer.

Figure 4. Time domain transmission measurement system with a FPGA.

mostly in the digital part behind the analog-digital converter (ADC); the front end was very similar.

A block diagram and a photograph of the first system using a microcontroller are shown in Figure 3. Two slightly detuned clocks are synthesized from a crystal. One clock triggers a step generator, which transmits a step signal with about 30ps rise time (20% to 80%) and up to 3V amplitude. The other triggers the track and hold amplifier (having an input bandwidth of 13GHz), the 12bit ADC, and the asynchronous FIFO (first in first out) memory with a width of 18bit and a depth of 32k. A microcontroller and a computer control the system. The FIFO memory can be read out, and the clock generation can be programmed via the I2C-bus. Clock signals up to hundreds of megahertz can be chosen with an accuracy of 1ppm. The dimensions of the RF-PCB are 90mm $\times$ 60mm. A reference path is necessary to measure time differences, because the phase of the two clock signals is not captured. A FIFO has to be used because the microcontroller is not able to read in 12bit words at tens of megahertz. Therefore, one waveform of up to 32k is captured at a time and is then transferred to the computer. Averaging, in order to improve the SNR, is carried out on the computer.

An improvement is the application of a field programmable gate array (FPGA). A modular system is shown in Figure 4. There is no more need for a fast external FIFO because data can be read into the FPGA directly up to about 66MHz. Furthermore, no reference path is needed, because the FPGA is able to discriminate the phase between both clock signals. Up to $2^{12} = 4096$ sampling points are possible while an averaging of up to $2^{13} = 8192$ waveforms can be carried out on the FPGA (this is restricted due to the internal resources of the FPGA used[2]).

Since both front ends are similar they offer a comparable performance. The RMS noise level of the receiver is < 0.9mV, the RMS jitter is < 0.7ps (no averaging). Figure 5 shows a comparison of sampled test signals between the proposed hardware and a Tektronix TDS8000. The frequencies are chosen as $f_1 = 50.01$MHz and $f_2 = 50$MHz, which leads to a resolution

[2] A Spartan 6 from Xilinx is used.

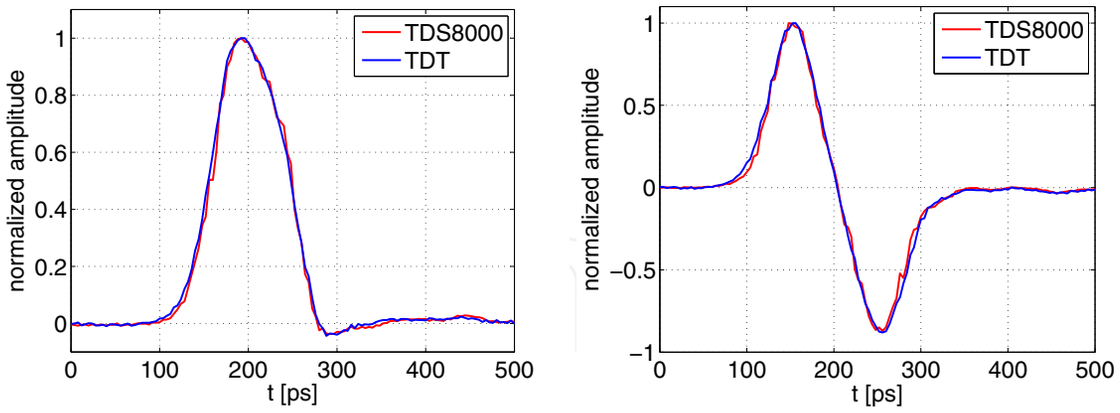

(a) Pulse. (b) Monocycle.

Figure 5. Comparison between the proposed dedicated hardware (TDT) and a Textronix TDS8000 (no averaging).

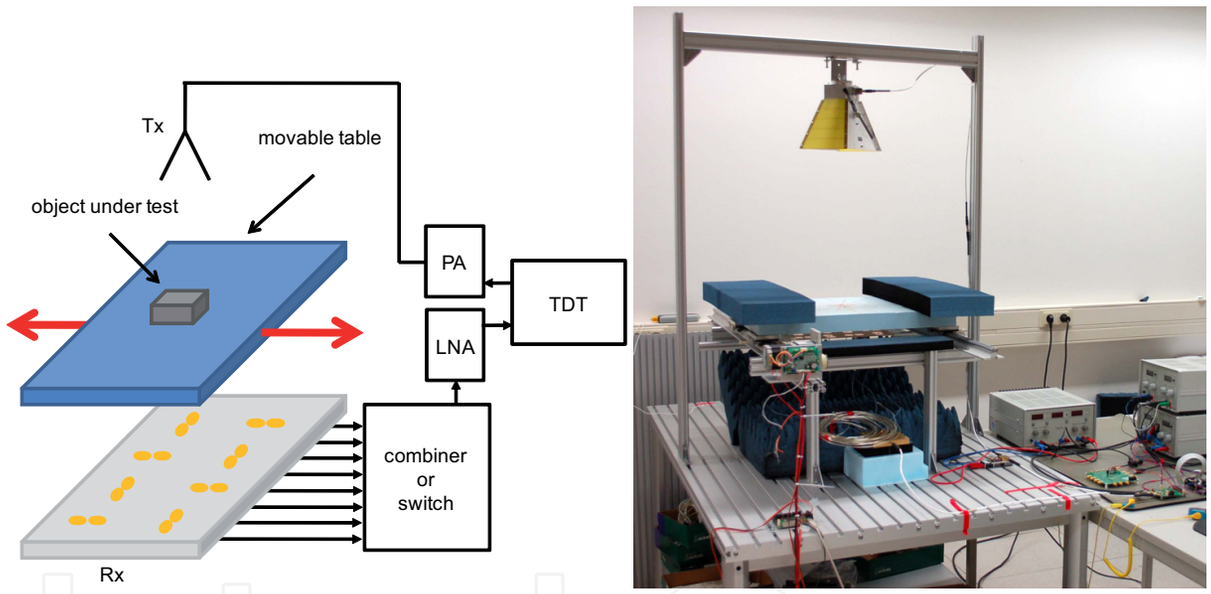

(a) Block diagram. (b) Photograph.

Figure 6. Entire measurement set-up.

of $\Delta T = 4$ps. For the measurements presented later a much lower resolution is sufficient, e.g. $\Delta T = 40$ps.

3.3. Entire measurement setup

The entire measurement system is shown is Figure 6. The step signal of the TDT is amplified by a power amplifier (PA) before being transmitted through a horn antenna. The object under test is illuminated by the transmitted signal and portions of the scattered signal are received by an array of eight receiving antennas, which are arranged in two orthogonal polarizations. In order to emulate a 2-dimensional array, the movable table is moved orthogonally to the orientation of the receiving array. It is crucial to the multivariate calibration, which is applied

later, that the received signals of each antenna placed at its unique position are sampled separately. Therefore, the antennas are switched sequentially onto the input of the TDT and are sampled there, after being amplified by a low noise amplifier (LNA). The MOSFET switch used requires relatively high hard- and software effort and it has to be synchronised with the other components included in the system. Furthermore, these switches have a latency of some nanoseconds. The switch has an insertion loss of 4dB at 2GHz and 8.6dB at 8GHz.

A simpler solution is to use a broadband combiner. The signals received by the individual antennas are combined using a broadband eight-way Wilkinson divider. Prior to combining there is a delay of $\tau = 2$ns between two adjacent inputs. It is possible to separate the individual pulses in time. Compared to using a receiver having more channels, or using a switch, the hardware effort is greatly reduced and the instantaneous sampling of all pulses is possible in about 20ns. One of the disadvantages that has to be considered is that there is an increased insertion loss of ideally 9dB; at 1GHz and 5GHz the measured insertion losses are 9.3dB and 10.7dB, respectively. There are also losses and temperature dependencies due to the delay lines, which have to be taken into account.

4. Measurements

For the multivariate analysis applied later it is necessary to measure a large number of objects varying in their dielectric and geometric properties. Here, two series of measurements are presented.

The first series comprised objects of moist clay granules. Five irregularly shaped moulds were manufactured from polystyrol foam[3]. They were then filled with clay granules having different amounts of moisture. One of the moulds is shown in Figure 7. The moisture content was varied in a range from about 4.5% to 24%[4] and reference measurements were carried out with a gravimetric method[5]. Furthermore, three rotation angles of 0°, 22.5° and 45° were applied to the test objects when putting them on the movable table in order to have more variation in the received signals. Overall 90 different objects were measured. The measurements were carried out in random order to avoid correlations with environmental effects, e.g. temperature variations.

Since there are eight receiving antennas and the movable table is moved to four positions, 32 pulses are received for every object under test when using a switch. With the Wilkison divider and delay lines, the pulses of the eight antennas are received instantaneously as a series of pulses. Two of the received series of pulses for two different objects having moisture contents of 4.88% and 20.93% are shown as examples in Figure 8. Although the variation in moisture content is high, the variation in the pulse shape is rather low.

The second series comprised plastic bottles filled with ethanol-water mixtures[6]. The water content was varied in a range from 2% to 20% in steps around 2%; reference measurements were carried out using a precision balance[7]. Ten bottles were filled with a total of around 190g

[3] In the following: *test series 1*

[4] All given moisture contents are on a wet basis.

[5] A Sartorius MA100 is used, accuracy of the weighing function: 0.1% for samples $>$ 1g and 0.02% for samples $>$ 5g. The weight of the samples was about $4 - 8$g.

[6] In the following: *test series 2*

[7] The gravimetric water content was determined using a Kern EW 4200-2NM. The repeatability is 0.01g.

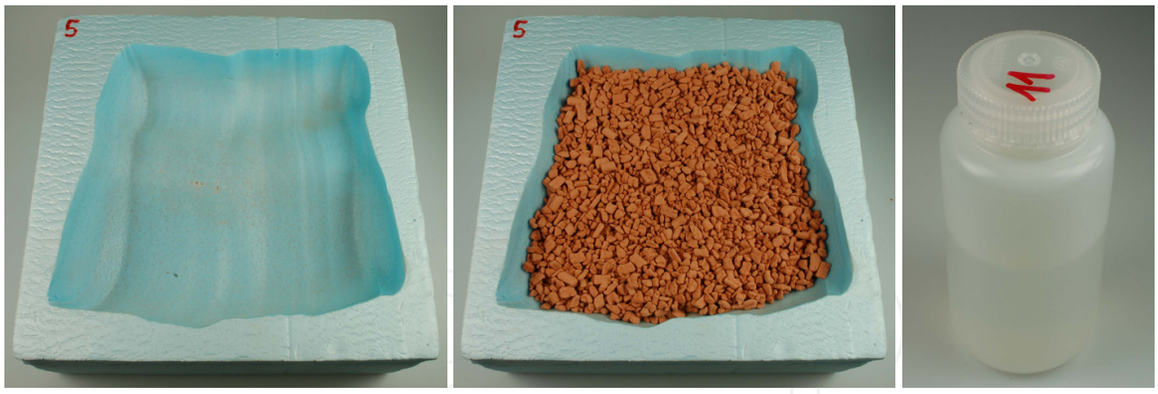

(a) One of the moulds manufactured from Styrofoam.

(b) Mould filled with moist clay granules.

(c) A bottle filled with an ethanol-water mixture.

Figure 7. Objects under test.

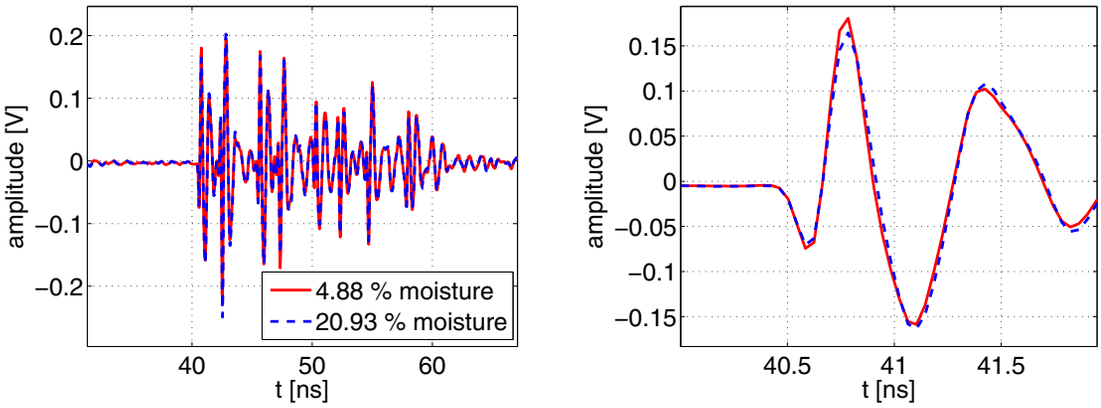

(a) Instantaneous sampled pulses received by the eight antennas using a broadband Wilkinson divider and delay lines.

(b) Closer look at the first received pulse.

Figure 8. Examples of received pulses from two objects having different moisture content.

of liquid, and another ten with about 140g. Therefore, overall 20 objects were measured. A photograph of one of the measured objects containing 113.15g ethanol and 27.94g of water is shown in Figure 7.

The time domain signals are gated in order to extract the time interval of interest: about 10 to 30 equidistant amplitude values per pulse are empirically chosen and subjected to the multivariate calibration methods which will be explained in the next section 5.

5. Multivariate data processing

The sequence of the eight sampled pulses consists of 217 sampling points. There are four positions of the movable table which then leads to $4 \times 217 = 868$ data points per object. These pulses are modified by many factors: the shape, the position, the rotation, and the intrinsic variables of the material under test. However, as can be seen in Figure 8 the value to be measured has only a relatively low influence on the apparent shape of the pulses, and

practically all data points are modified when one or more of the factors mentioned above changes. Indeed each factor modifies the curve shape in a different manner. Therefore all measured points of the curve contribute in part to the variable(s) to be measured. Often these values consist only of one variable (for instance water content), a small set of variables (complex permittivity, quality) or an abstract class (shape of the object). Hence the challenge of data processing for the application discussed here is to extract the (hidden) relevant information from a huge data array. Due to the complexity physical modelling is impracticable.

Multivariate calibrations are established techniques for the extraction of relevant information from observed (measured) data without physical modelling. In the following, principal components analysis and regression (PCA/PCR), artificial neural networks (ANN) and partial least squares regression (PLSR) are applied to the data measured during the experiments described in section 4. Multivariate calibration methods have the disadvantage that they require a calibration procedure i.e. training. This means a portion of the measurements carried out on known samples need to be used to determine parameters or coefficients that enable a determination of the variable to be measured for unknown samples.

For this reason the measurements are divided randomly into a calibration and validation group. In general these two groups have an equal size. For test series 1 the number of data sets of the calibration and validation groups is $n_c = n_v = 45$ and for test series 2 they are $n_c = n_v = 10$. The more samples are available the more robust is the calibration and the meaningfulness of the validation.

In order to reduce the amount of data, in a pre-processing step the points having a lower variance may be removed from the input variables. For the experiments described here a majority of the 868 time points can be neglected when the threshold value of the standard deviation is set to 20% of the maximum standard deviation[8]. Thus for test series 1 and 2 the number of points used is $m_1 = 305$ and $m_2 = 187$, respectively. The raw matrix of the calibration data consists of the measured and pre-processed pulse sequence in each line. Hence the columns contain the data of the selected time points of a measurement:

$$Y_c = \begin{bmatrix} y_{11} & \cdots & y_{1m} \\ \vdots & \ddots & \vdots \\ y_{n_c 1} & \cdots & y_{n_c m} \end{bmatrix}. \tag{2}$$

Due to numerical reasons it is advantageous to standardize the raw data. Firstly the means of each column are calculated with

$$\overline{Y}_c = \left[\frac{1}{n_c} \sum_{i=1}^{n_c} y_{i1} \cdots \frac{1}{n_c} \sum_{i=1}^{n_c} y_{im} \right]. \tag{3}$$

The matrix of the normalized, standardized calibration data is calculated by subtracting the means of each column from each value of the columns, then dividing each by the standard deviations of the columns $\sigma_{c1} \cdots \sigma_{cm}$:

$$X_c = \left[Y_c - \begin{bmatrix} 1 \\ \vdots \\ 1 \end{bmatrix} \cdot \overline{Y}_c \right] \cdot \begin{bmatrix} \frac{1}{\sigma_{c1}} & \cdots & 0 \\ \vdots & \ddots & \vdots \\ 0 & \cdots & \frac{1}{\sigma_{cm}} \end{bmatrix}. \tag{4}$$

[8] which is 0.0037 and 0.0017 for test series 1 and 2, respectively.

The matrix of the pre-processed validation data is calculated similarly. However the data is normalized and standardized using the means and the standard deviations of the calibration set.

5.1. Principal component analysis and regression

As can be seen in Figure 8 neighbouring data points are highly correlated. Therefore it is not possible to use the selected data points directly in a linear regression to estimate the variable of interest[9]. For the two test series described in section 4 such a linear calibration equation would have $m_1 = 305$ and $m_2 = 187$ coefficients. Furthermore, and this aspect is more relevant, the calculation of the coefficients is numerically unstable because a matrix with correlated data needs to be inverted in the regression algorithm.

A solution to this problem is found using principal component analysis (PCA). The original data is linear transformed into a new set of variables

$$H_c = X_c \cdot P. \tag{5}$$

H_c comprises the so called principal components (the scores) and P is a matrix of the so called loadings. The scores have the advantage that they are uncorrelated and are arranged in such a way that the first principal component has the highest variance and the others are arranged in decreasing order of variance.

The matrix of the loadings P is composed of the eigenvectors. They are also orthogonal and of unit length. This transformation can be interpreted as a transformation into a new orthogonal coordinate system. The basis vectors of the new coordinate system are the eigenvectors and their direction is along the variances in decreasing order.

The properties of the principal components, their orthogonality and their arrangement regarding the variance, enable data reduction because the relevant information of the matrix is already described by the first few principal components. In order to obtain the properties of the transformed data as described above, the matrix P needs to be calculated by an eigenvalue decomposition [36–38] but this is not described in detail here. For the results calculated here the statistical toolbox of MATLAB is used. The eigenvalue decomposition of the PCA is processed without any consideration of the variable(s) of interest. This will be done in the next step of the data processing.

As mentioned above a multiple linear regression of the untransformed (therefore correlated) data is numerically unstable, but after the transformation (see eq. (5)) the data is uncorrelated and the value to be determined can be estimated by a linear combination of the principal components (principal component regression, PCR):

$$\hat{z_c} = \tilde{H_c} \cdot \beta, \tag{6}$$

where $\hat{z_c}$ is the estimated variable of interest (objective variable), $\tilde{H_c}$ is the matrix of the selected principal components and the vector β contains the coefficients of the linear equation.

[9] The variable of interest or objective variable is the parameter to be determined later, e.g. the moisture content.

The entries in the first column of $\tilde{H}_c$ are all unity in order to describe the mean of the value of interest in the linear equation.

In $\tilde{H}_c$ only the first k principal components are included. This selection leads to the desired data reduction. The value k need to be determined heuristically. Here for test series 1 the number of principal components used is $k_1 = 12$ and for test series 2 it is $k_2 = 2$.

The coefficients of the linear equation can be calculated by the following equation:

$$\beta = \left(\tilde{H_c}^T \cdot \tilde{H_c}\right)^{-1} \cdot \tilde{H_c} \cdot z_c, \tag{7}$$

where z_c consists of the variable of interest determined by a reference method, e.g. oven drying for moisture content.

After the calibration data is processed the system is essentially calibrated and is ready to handle unknown samples. However prior to that, the performance of the calibration still needs to be evaluated using the validation data. The target variables of interest are also determined for the pre-processed validation data using a reference method. The validation data (or later in use, the data of a measurement of an unknown sample) is processed in the following manner:

1. the scores are estimated using the loadings determined during the calibration procedure: $\hat{H_v} = X_v \cdot P$,
2. the unused principal components are removed and the unit column is added: $\hat{H_v} \Rightarrow \tilde{\hat{H}}_v$,
3. the value of interest is estimated by the linear equation $\hat{z_v} = \tilde{\hat{H}}_v \cdot \beta$.

For the evaluation of the quality of the calibration the root mean square error of calibration group $RMSE_c$ and the validation group $RMSE_v$ are calculated.

The results obtained with PCA/PCR for both test series are shown in Figure 9. The predicted moisture or water content is plotted vs. its true values. With perfect prediction all points of

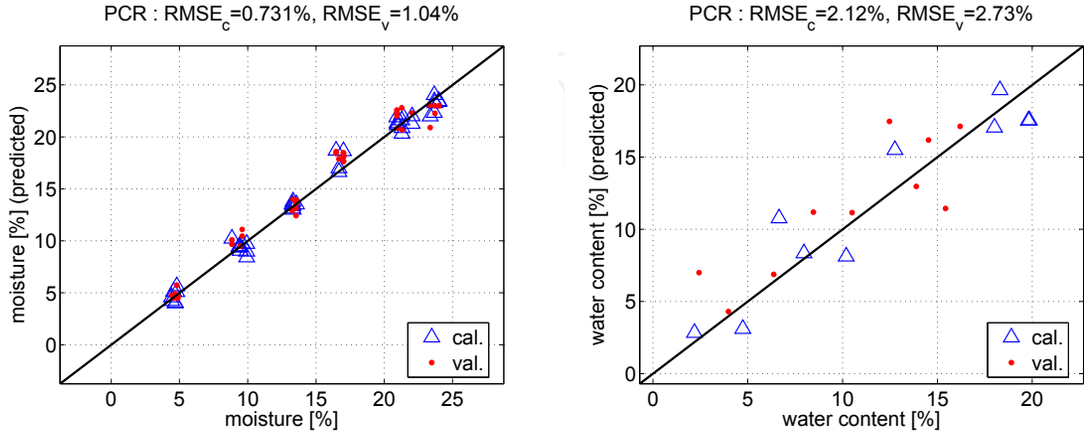

(a) Test series 1: clay granules.

(b) Test series 2: ethanol-water mixtures.

Figure 9. Results obtained with PCA/PCR for both test series.

RER	Classification	Application
Up to 6	Very poor	Not recommended
7-12	Poor	Very rough screening
13-20	Fair	Screening
21-30	Good	Quality control
31-40	Very good	Process control
41+	Excellent	Any application

Table 1. *Classification using RER-values according to [39].*

the calibration and validation group would be on the so called quality line. For test series 1 a $RMSE_c = 0.731\%$ and $RMSE_v = 1.04\%$ is achieved. For test series 2 the errors are $RMSE_c = 2.12\%$ and $RMSE_v = 2.73\%$. The meaningfulness of $RMSE$ depends on the range of the variable to be predicted. Therefore the range error ratio RER is a better choice to evaluate the calibration. It is the ratio between the variable range $\Delta z = \max z - \min z$ and the RMSE[10]:

$$RER = \frac{\Delta z}{RMSE}. \tag{8}$$

The quality of the performance can be assessed using the ranges suggested in Table 1. For test series 1 the $RER_c = 26.7$ and $RER_v = 18.75$, hence the performance is *good*. But for test series 2 the accuracy obtained with PCA/PCR is only *poor* because $RER_c = 8.5$ and $RER_v = 6.6$.

5.2. Artificial neural networks

Although PCA/PCR is a linear operation it is more or less capable of processing non-linear data. However, when the unknown function describing the relationship between the pulse sequence and the value of interest is non-linear a purely linear method may not be the best choice. Artificial neural networks (ANN) can approximate unknown non-linear functions. For this application multilayer-feed-forward (MLFF) networks have a suitable architecture [40].

Such a network is shown in Figure 10. The input variables are weighted and processed by the neurons of the hidden layer. The activation functions of the neurons are non-linear[11]. This enables the non-linear function approximation. The output variable of the hidden layer is weighted again and processed by the neuron(s) of the output layer. The output of this layer needs to be post-processed (scaling and mean value) and the estimated variable of interest is available.

Due to their architecture ANN have several degrees of freedom: the number of hidden layers, the kind of activation function in each layer, and the number of neurons in the hidden layer. For the application discussed here one hidden layer and $n_{HL} = 10$ neurons in this hidden layer are sufficient. The problem is that the number of weighting factors between the layers increases with the number of neurons and for an optimal determination of the weighting factors a relatively large number of samples for the calibration (training) is necessary.

[10] In [39] the standard error is used instead of the root mean square error; for large numbers of samples there is practically no difference.

[11] tansig-function

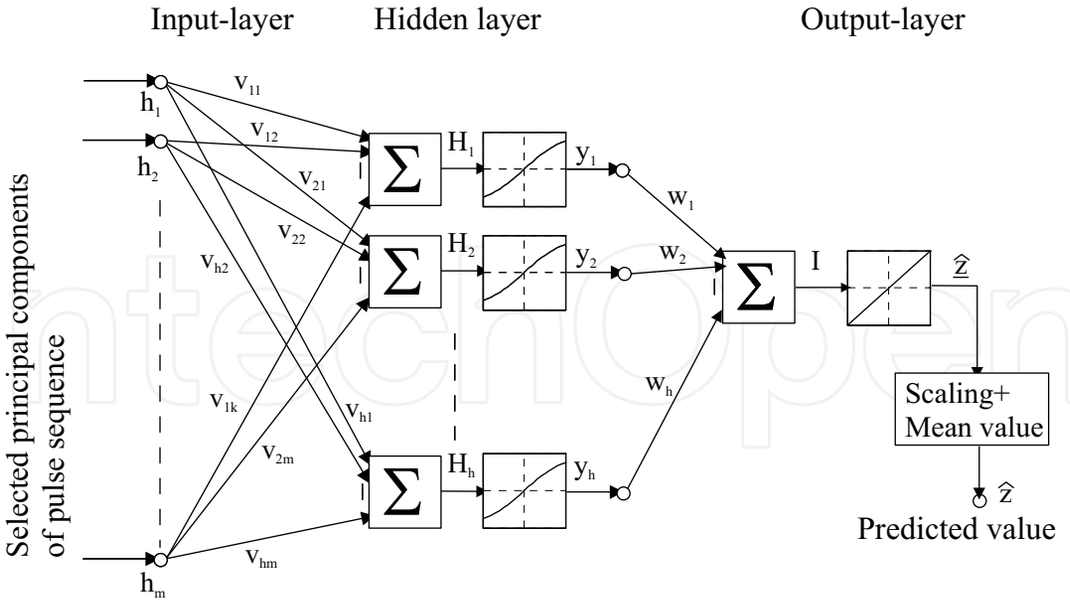

Figure 10. Architecture of the used multilayer-feed-forward-ANN.

For this reason a pre-processing of the data is recommended. If all selected time points were to be fed into the input layer $m_1 n_{HL} = 3050$ and $m_2 n_{HL} = 1870$ weighting factors would need to be found, with only $n_c = 45$ (test series 1) $n_c = 10$ training data sets. Therefore it is useful to feed the ANN with the selected principal components because they include the relevant information. This means the linear principal components regression is replaced by the non-linear ANN.

The training of the ANN has a relatively high calculation effort. Furthermore the starting values for the weighting factors are set randomly at the beginning of the training. This means the method is not strongly deterministic and it is not known for example, whether the optimal weighting factors were found because the training stopped in a local minimum of the error function. The training of the ANN was effected using the artificial neural network toolbox of MATLAB.

The results of the ANN are plotted in Figure 11. In comparison to the results of PCA/PCR there is an improvement observable:

- for test series 1 the RER_c increases to 37.8 (rating: *very good*) and the $RER_v = 22.4$ (*good*). This means there is a slight overfitting,
- for test series 2 the following ratings are obtained: $RER_c = 25.5$ (*good*) and $RER_v = 18.1$ (*fair*).

Despite the much higher calculation effort of ANN the improvements are not very satisfactory.

5.3. Partial least squares regression

PCA decorrelates the data by eigenvalue decomposition. Therefore the variable(s) of interest are not considered in this procedure. Only at the stage of PCR are they taken into account and a selection of relevant principal components is necessary. With the partial-least-squares

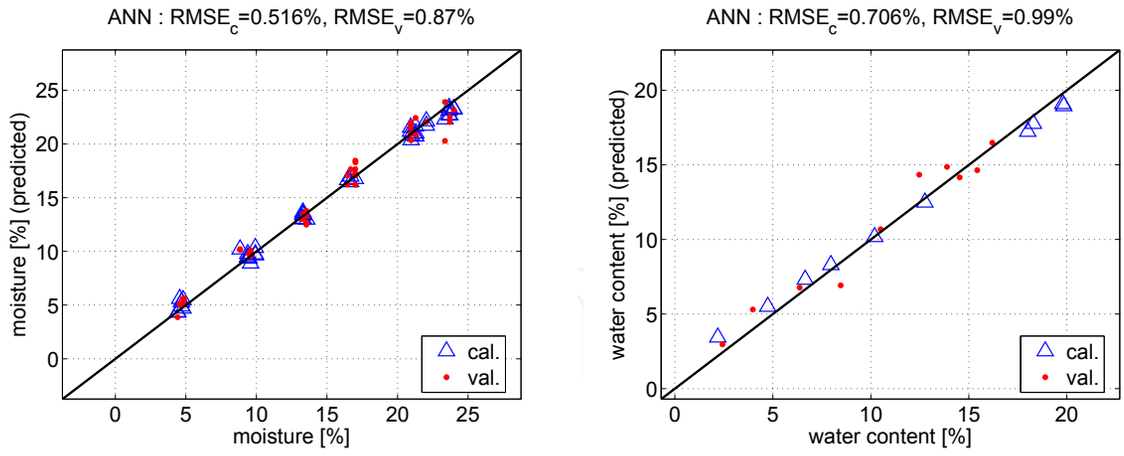

(a) Test series 1: clay granules.

(b) Test series 2: ethanol-water mixtures.

Figure 11. Results obtained with ANN for both test series.

regression (PLSR) the data is decorrelated regarding the variables(s) of interest. Several PLSR algorithms exist and sometimes the data is pre-processed non-linearly. Although PLSR was developed, more or less intuitively, in order to analyze economic data, in the meantime this method has also been used for several applications in other fields.

The algorithm used here for the processing of the measured data is described in [7] in detail and is only summarized in the following.

- Firstly, the input values are weighted in such a way that the covariance between them and the variable of interest is maximal.
- Secondly, the projection of the input values on the vector of the weighting values is called a *factor* or a *hidden path variable*. In the following, two regression analyses are considered:
  1. between the input variables and the factor, and
  2. between the variable of interest and the factor.

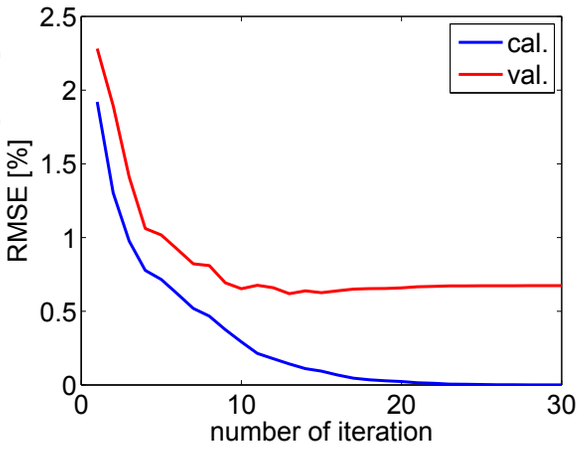

Figure 12. Influence of the number of factors H on the performance of the PLSR.

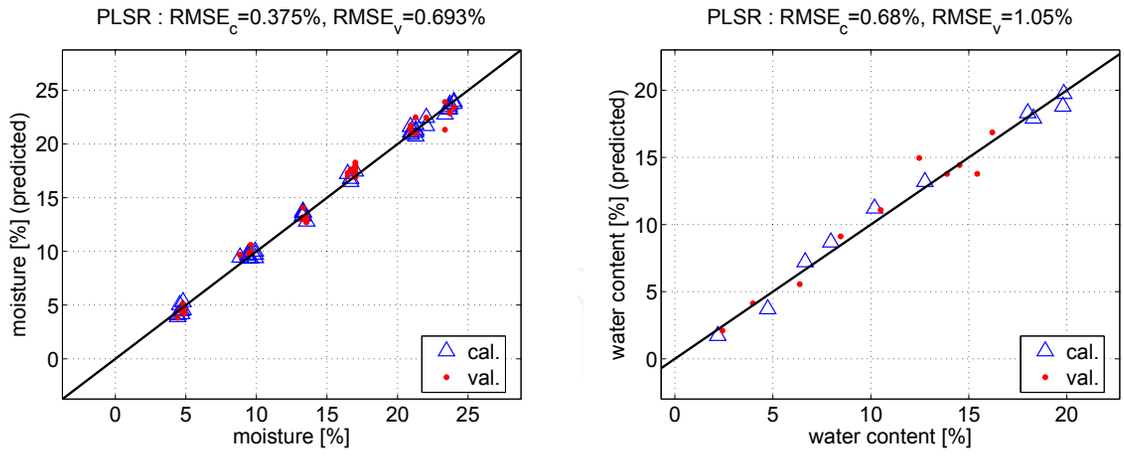

(a) Test series 1: clay granules.

(b) Test series 2: ethanol-water mixtures.

Figure 13. Results obtained with PLSR for both test series.

- Thirdly, the parts described by these linear models are subtracted from the measured values and the variables of interest and the algorithm is restarted using this new data in order to calculate the next factor,
- and finally, the procedure is repeated iteratively until a specified number H of hidden path variables is calculated.

All determined regression coefficients and weighting factors are used finally for the calculation of the regression equation. This means for the validation (and later application) that only a linear combination of the input values need to be calculated. Hence the calculation effort is much smaller in comparison to the ANN. The only degree of freedom is H, the number of factors to be used (number of iterations). When H is too high the $RMSE_c$ is significantly smaller than the $RMSE_v$. This means that overfitting occurs. However, as shown in Figure 12 H should be selected where $RMSE_v$ has a minimum. Furthermore $RMSE_c$ should not be much smaller (factor 1/2) than $RMSE_v$, otherwise the PLSR calibration could not handle unknown samples.

The performance of the PLSR is shown in Figure 13. For test series 1 $RER_c = 52$ (*excellent*) and $RER_v = 28.1$ (*good*). This is a further improvement in comparison to the ANN. For test series 2 the results stay similar to those of ANN: $RER_c = 26.5$ (*good*) and $RER_v = 17.1$ (*fair*).

5.4. Best calibration method

Principal component analysis and regression lead to acceptable results but the best calibrations were obtained with ANN and PLSR. However the computation effort is much higher with ANN and in general more samples are necessary for a successful training. PLSR is a linear operation and can be performed fast in real time. For this reason PLSR is the best choice for calibration of the application discussed here. In Table 2 the results of both test series are compared with similar experiments presented in several other publications. As can be seen, the performance obtained here is in the upper range. However one has to take into account the further advantages of the system discussed here: it is non-contacting, the objects can be rotated, and can have irregular shapes and sizes.

Publication	range [%]	$RMSE_c$ [%]	$RMSE_v$ [%]	RER_c	RER_v
[41]: Tobacco, PLSR	10-50	-	2	-	20
[42]: Scots pine, PLSR	0-15	0.46	0.74	32.6	20.3
[42]: Scots pine, PLSR	0-175	15.92	12.52	11	14
[9]: Clay granules, ANN	6.3-34.2	1.6	2.1	17.4	13.3
ISOperm:					
Clay granules, PLSR	4.5-24	0.38	0.69	52	28.1
Ethanol water mix. in bottle, ANN	2-20	0.71	1	25.5	18.1
[14], PLSR	70-100	1.28	2.55	23.4	11.8
[16], ANN	5-29.2	1.29	1.88	18.8	12.9
[17], PLSR	4.6-24.1	0.35	0.69	55.3	28.2
[19], PLSR	1.8-20.2	0.39	0.61	47.3	30.2
[20], PLSR	4.3-23.4	0.31	0.55	61.7	34.7
Other technologies:					
[43]: Wheat, admittance, PCR	9-20	-	0.39	-	28.2
[44]: Salmon, NIR, PLSR	61-70.8	-	0.98	-	10
[45]: Paper, NIR, PLSR	0-2.4	-	0.056	-	43.1
[46]: Theophyllin, NIR, ANN	1-22	0.45	0.83	46.7	25.3

Table 2. Comparison to other publications regarding the accuracy of the determination of moisture or water content. Except the method investigated in ISOPerm, all others are contacting and/or require a defined shape of the object under test.

6. Conclusions

Many industrial and scientific applications require extensive on-line process monitoring and quality control. Often the composition of goods (e.g. moisture content) is of great interest but also abstract parameters, for example quality or freshness, play an important role. The microwave sensor described is able to penetrate the investigated materials and by using UWB-techniques it is possible to gain information at various frequencies. The applied time domain techniques operate with low hardware effort and fast measurement speed while having a high accuracy. Using commercial MMICs signals exceeding a bandwidth of 10GHz can be generated and sampled with cheap and compact dedicated hardware. Today it is possible to employ multivariate calibration methods like artificial neural networks, which have a high computational effort, in real time. These methods are well established in, for example, NIR or image processing and are successfully adopted. The feasibility of the method has been successfully proven with accuracy even greater than in many previous publications using contacting methods. It has a great potential for many kinds of future applications in microwave sensing.

Author details

Henning Mextorf, Frank Daschner, Mike Kent and Reinhard Knöchel
University of Kiel, Germany

7. References

[1] Vainikainen, P. & Laitinen, T. [2009]. *Proceedings of the 8th International Conference on Electromagnetic Wave Interaction with Water and Moist Substances (ISEMA 2009)*, Espoo, Finland.

[2] Grant, E. H., Sheppard, R. J. & South, G. P. [1978]. *Dielectric behaviour of biological molecules in solution*, Clarendon Press, Oxford, UK.

[3] Fellner-Feldegg, H. [1969]. The measurement of dielectrics in the time domain, *J. Phys. Chem.* 73: 616 – 623.

[4] Burdette, E., Cain, F. & Seals, J. [1980]. In vivo probe measurement technique for determining dielectric properties at VHF through microwave frequencies, *IEEE Trans. Microw. Theory Tech.* 28(4).

[5] Kent, M. & Anderson, D. [1996]. Dielectric studies of added water in poultry meat and scallops, *Journal of food engineering* 28(3-4): 239–259.

[6] Kent, M., Knöchel, R., Daschner, F. & Berger, U.-K. [2000]. Composition of foods using microwave dielectric spectra, *Eur. Food Res. Technol.* (210): 359–366.

[7] Martens, H. & Naes, T. [1989]. *Multivariate Calibration*, John Wiley and Sons, Chichester.

[8] Kent, M., Knöchel, R., Daschner, F., Schimmer, O., Oelenschläger, J., Mierke-Klemeyer, S., Barr, U.-K., Floberg, P., Huidobro, M., Nunes, L., Batista, I. & Martins, A. [2004]. Time domain reflectometry as a tool for the estimation of quality in foods, *Agrophysics* 18(3).

[9] Schimmer, O., Gülck, A., Daschner, F., Piotrowski, J. & Knöchel, R. [2005]. Non-contacting determination of moisture content in bulk materials using sub-nanosecond UWB-pulses, *IEEE Trans. Microw. Theory Tech.* 53(6): 2107–2113.

[10] Mextorf, H., Martens, R., Daschner, F. & Knöchel, R. [2010]. Dual polarized UWB antenna for free-space characterization of dielectric objects, *Proc. German Microwave Conference 2010* pp. 162 – 165.

[11] Mextorf, H., Daschner, F., Kent, M. & Knöchel, R. [2010a]. Free-space determination of permittivity, size and orientation of rectangular shaped objects using multivariate analysis, *Proc. European Microwave Conference 2010* pp. 152 – 155.

[12] Mextorf, H., Daschner, F., Kent, M. & Knöchel, R. [2010b]. Non-contacting UWB-characterization of dielectric objects using multivariate calibration, *Proc. Aquametry 2010* pp. 136 – 144.

[13] Mextorf, H., Daschner, F., Kent, M. & Knöchel, R. [2011d]. UWB free-space characterization and shape recognition of dielectric objects using statistical methods, *IEEE Trans. Instrum. Meas.* 60(4): 1389 – 1396.

[14] Mextorf, H., Daschner, F., Kent, M. & Knöchel, R. [2011a]. Free-space prediction of the water content of irregularly shaped bodies filled with water-ethanol mixtures, *Proc. ISEMA 2011* pp. 162 – 169.

[15] Mextorf, H., Daschner, F., Kent, M. & Knöchel, R. [2011b]. New UWB free-space method for the classification and characterization of dielectric objects, *Proc. ICUWB 2011* pp. 410–414.

[16] Mextorf, H., Daschner, F., Kent, M. & Knöchel, R. [2011c]. Performance of multivariate calibration methods for the UWB characterization of dielectric objects, *Proc. CMM-Tagung 2011* pp. 105–112.

[17] Mextorf, H., Daschner, F., Kent, M. & Knöchel, R. [2012a]. Non-contacting moisture sensing using a dedicated UWB time domain instrument, *Proc. German Microwave Conference 2012* pp. 1–4.

[18] Mextorf, H., Daschner, F., Kent, M. & Knöchel, R. [2012b]. Signal quality considerations for free-space UWB moisture measurements, *Proc. Mikon 2012* pp. 627–630.
[19] Mextorf, H., Daschner, F., Kent, M. & Knöchel, R. [2012c]. UWB time domain transmission sensor for free-space moisture measurements, *IEEE MTT-S Int. Microw. Symp. Dig. 2012* pp. 1–3.
[20] Mextorf, H., Sachs, J., Daschner, F., Kent, M. & Knöchel, R. [2012]. Free-space moisture prediction of small objects using M-sequences, *Proc. ICUWB 2012* pp. 260–264.
[21] Schantz, H. G. [2003a]. Introduction to ultra-wideband antennas, *IEEE Conference on Ultra Wideband Systems and Technologies* pp. 1–9.
[22] Schantz, H. G. [2003b]. UWB magnetic antennas, *IEEE Antennas and Propagation Society International Symposium* 3: 604–607.
[23] Schantz, H. G. [2004]. A brief history of UWB antennas, *IEEE Aerospace and Electronic Systems Magazine* 19(4): 22–26.
[24] Schantz, H. G. [2005]. *The Art and Science of Ultrawideband Antennas*, Artech House, Norwood, MA.
[25] Wiesbeck, W., Adamiuk, G. & Sturm, C. [2009]. Basic properties and design principles of UWB antennas , *IProceedings of the IEEE* 97(2): 372–385.
[26] Perruisseau-Carrier, J., Hee, T. W. & Hall, P. S. [2003]. Dual-polarized broadband dipole, *IEEE Antennas Wireless Propag. Lett.* 2(1): 310–312.
[27] Woten, D. A. & El-Shenawee, M. [2008]. Broadband dual linear polarized antenna for statistical detection of breast cancer, *IEEE Trans. Antennas Propag.* 56(11): 3576–3590.
[28] Teo, P.-T., Lee, K.-S. & Lee, C.-K. [2003]. Maltese-cross coaxial balun-fed antenna for GPS and DCS1800 mobile communication, *IEEE Trans. Veh. Technol.* 52(4): 779–783.
[29] Suh, S.-Y., Stutzman, W., Davis, W., Walthot, A. & Schiffer, J. [2004]. A generalized crossed dipole antenna, the fourtear antenna, *IEEE APS 2004* 3: 2915–2918.
[30] Mak, K.-M., Wong, H. & Luk, K.-M. [2007]. A shorted bowtie patch antenna with a cross dipole for dual polarization, *IEEE Antennas Wireless Propag. Lett.* 6: 126–129.
[31] Adamiuk, G., Beer, S., Wiesbeck, W. & Zwick, T. [2009]. Dual-orthogonal polarized antenna for UWB-IR technology, *IEEE Antennas Wireless Propag. Lett.* 8: 981–984.
[32] Soroka, S. [1986]. A physically compact quad ridge horn design, *IEEE APS 1986* pp. 903–906.
[33] Shen, Z. & Feng, C. [2005]. A new dual-polarized broadband horn antenna, *IEEE Antennas and Wireless Propagation Letters* 4: 270–273.
[34] Schaubert, D., Elsallal, W., Kasturi, S., Boryssenko, A., Vouvakis, M. N. & Paraschos, G. [2008]. Wide bandwidth arrays of vivaldi antennas, *Institution of Engineering and Technology Seminar on Wideband, Multiband Antennas and Arrays for Defence or Civil Applications* pp. 1–20.
[35] Adamiuk, G., Zwick, T. & Wiesbeck, W. [2007]. Dual-orthogonal polarized vivaldi antenna for ultra wideband applications, *MIKON 2008* pp. 1–4.
[36] Götze, J. [1989]. *Orthogonale Matrizentransformationen*, R. Oldenbourg Verlag, München.
[37] G. Engeln-Muellges, F. R. [1996]. *Numerik Algorithmen*, VDI-Verlag, Düsseldorf.
[38] G.H. Golub, v. L. [1996]. *Matrix Computations*, The John Hopkins University Press, Baltimore.
[39] Williams, P. C. [2001]. *Near-Infrared Technology in the Agriculture and Food industries*, 2nd edn, American Association of Cereal Chemists, Inc., chapter Implementation of near-infrared technology, p. 165.
[40] Patterson, D. [1997]. *Künstliche neuronale Netze*, Prentice Hall Verlag, Haar.

[41] Dane, A. D., Rea, G. J., Walmsley, A. D. & Haswell, S. J. [2001]. The determination of moisture in tobacco by guided microwave spectroscopy and multivariate calibration, *Analytica Chimica Acta* 429(2): 185–194.

[42] Johansson, J., Hagmana, O. & Oja, J. [2003]. Predicting moisture content and density of Scots pine by microwave scanning of sawn timber, *Computers and Electronics in Agriculture* 41(1-3): 85–90.

[43] Lawrence, K. C., Windham, W. R. & Nelson, S. O. [1998]. Wheat moisture determination by 1- to 110-MHz swept-frequency admittance measurements, *Transactions of the ASAE* 41(1): 135–142.

[44] Wold, J. P. & Isaksson, T. [1997]. Non-destructive determination of fat and moisture in whole atlantic salmon by near-infrared diffuse spectroscopy, *Journal of Food Science* 62(4): 734–736.

[45] Neimanis, R., Lennholm, H. & Eriksson, R. [1999]. Determination of moisture content in impregnated paper using near infrared spectroscopy, *1999 Annual Report Conference on Electrical Insulation and Dielectric Phenomena* 1: 162–165.

[46] Rantanen, J., Rasanen, E., Antikainen, O., Mannermaa, J.-P. & Yliruusi, J. [2001]. In-line moisture measurement during granulation with a four-wavelength near-infrared sensor: an evaluation of process-related variables and a development of non-linear calibration model, *Chemometrics and Intelligent Laboratory Systems* 56(1): 51–58.

IntechOpen